AGU PUBLICATIONS

JGR

Journal of Geophysical Research: Atmospheres

RESEARCH ARTICLE
10.1002/2016JD025109

Key Points:
- The seasonal cycle amplitude (SCA) of CO_2 roughly follows isentropic surfaces
- Changes in lower-latitude seasonal fluxes impact the SCA more than changes in higher-latitude fluxes
- The seasonality of the circulation can account for 10–20% of the SCA of an idealized CO_2 tracer

Correspondence to:
E. A. Barnes,
eabarnes@atmos.colostate.edu

Citation:
Barnes, E. A., N. Parazoo, C. Orbe, and A. S. Denning (2016), Isentropic transport and the seasonal cycle amplitude of CO_2, *J. Geophys. Res. Atmos.*, *121*, 8106–8124, doi:10.1002/2016JD025109.

Received 16 MAR 2016
Accepted 18 JUN 2016
Accepted article online 25 JUN 2016
Published online 12 JUL 2016

Isentropic transport and the seasonal cycle amplitude of CO_2

Elizabeth A. Barnes[1], Nicholas Parazoo[2,3], Clara Orbe[4,5], and A. Scott Denning[1]

[1]Department of Atmospheric Science, Colorado State University, Fort Collins, Colorado, USA, [2]Jet Propulsion Laboratory, California Institute of Technology, Pasadena, California, USA, [3]Joint Institute for Regional Earth System Science and Engineering, University of California, Los Angeles, California, USA, [4]Department of Earth and Planetary Sciences, Goddard Earth Sciences Technology and Research (GESTAR)/Johns Hopkins University, Baltimore, Maryland, USA, [5]NASA Goddard Space Flight Center, Greenbelt, Maryland, USA

Abstract Carbon-concentration feedbacks and carbon-climate feedbacks constitute one of the largest sources of uncertainty in future climate. Since the beginning of the modern atmospheric CO_2 record, seasonal variations in CO_2 have been recognized as a signal of the metabolism of land ecosystems, and quantitative attribution of changes in the seasonal cycle amplitude (SCA) of CO_2 to ecosystem processes is critical for understanding and projecting carbon-climate feedbacks far into the 21st Century. Here the impact of surface carbon fluxes on the SCA of CO_2 throughout the Northern Hemisphere troposphere is investigated, paying particular attention to isentropic transport across latitudes. The analysis includes both a chemical transport model GOES-Chem and an idealized tracer in a gray-radiation aquaplanet. The results of the study can be summarized by two main conclusions: (1) the SCA of CO_2 roughly follows surfaces of constant potential temperature, which can explain the observed increase in SCA with latitude along pressure surfaces and (2) increasing seasonal fluxes in lower latitudes have a larger impact on the SCA of CO_2 throughout most of the troposphere compared to increasing seasonal fluxes in higher latitudes. These results provide strong evidence that recently observed changes in the SCA of CO_2 at high northern latitudes (poleward of 60°N) are likely driven by changes in midlatitude surface fluxes, rather than changes in Arctic fluxes.

1. Introduction and Motivation

Carbon-concentration feedbacks and carbon-climate feedbacks constitute one of the largest sources of uncertainty in future climate [*Gregory et al.*, 2009]. Land CO_2 uptake by ecosystem production is enhanced by CO_2 fertilization [*Luo et al.*, 2006], but CO_2 release due to decomposition is enhanced by warming [*Hopkins et al.*, 2012]. Changes in nutrient cycling [*LeBauer and Treseder*, 2008] and land use [*Shevliakova et al.*, 2009] alter seasonal and long-term carbon storage on land. Long-term warming and drought also change the distribution of vegetation [*Cramer et al.*, 2001] and may contribute to substantial losses of carbon from biomass in forests [*Cox et al.*, 2004] and permafrost [*Schuur et al.*, 2013]. Terrestrial carbon cycle models show substantial differences in the magnitude and (at times) sign of the impact that these various ecosystem processes have had over recent decades on the atmospheric CO_2 budget [*Huntzinger et al.*, 2013; *Fisher et al.*, 2014b; *Tian et al.*, 2015]. Uncertainty in the future of carbon-climate feedbacks on land accounts for more than 2 W/m^2 of radiative forcing given identical top-of-atmosphere forcing among coupled carbon-climate models used in the Fifth Assessment of the Intergovernmental Panel on Climate Change [*Arora et al.*, 2013; *Wenzel et al.*, 2014; *Hoffman et al.*, 2014].

The seasonal cycle of near-surface CO_2 from the NOAA Marine Boundary Layer Reference data set (see section 2.1 for details) is shown in Figure 1a and exhibits enhanced concentrations in the cool season due to soil respiration and decreased concentrations in the warm season due to net uptake by the biosphere. Quantitative attribution of changes in the seasonal cycle amplitude (SCA; peak to trough differences in Figure 1a) of CO_2 to ecosystem processes is critical for testing models of carbon-climate feedback in the 21st century. Since the beginning of the modern atmospheric CO_2 record, seasonal variations have been recognized as a signal of the metabolism of land ecosystems [*Keeling*, 1960]. The quantitative relationship between SCA and its underlying biological drivers has been studied using tracer transport models since the 1980s [*Pearman and Hyson*, 1980; *Fung et al.*, 1983, 1987; *Randerson et al.*, 1997]. The SCA of CO_2 has been increasing for decades across the Northern Hemisphere, and this amplification has long been attributed to intensification

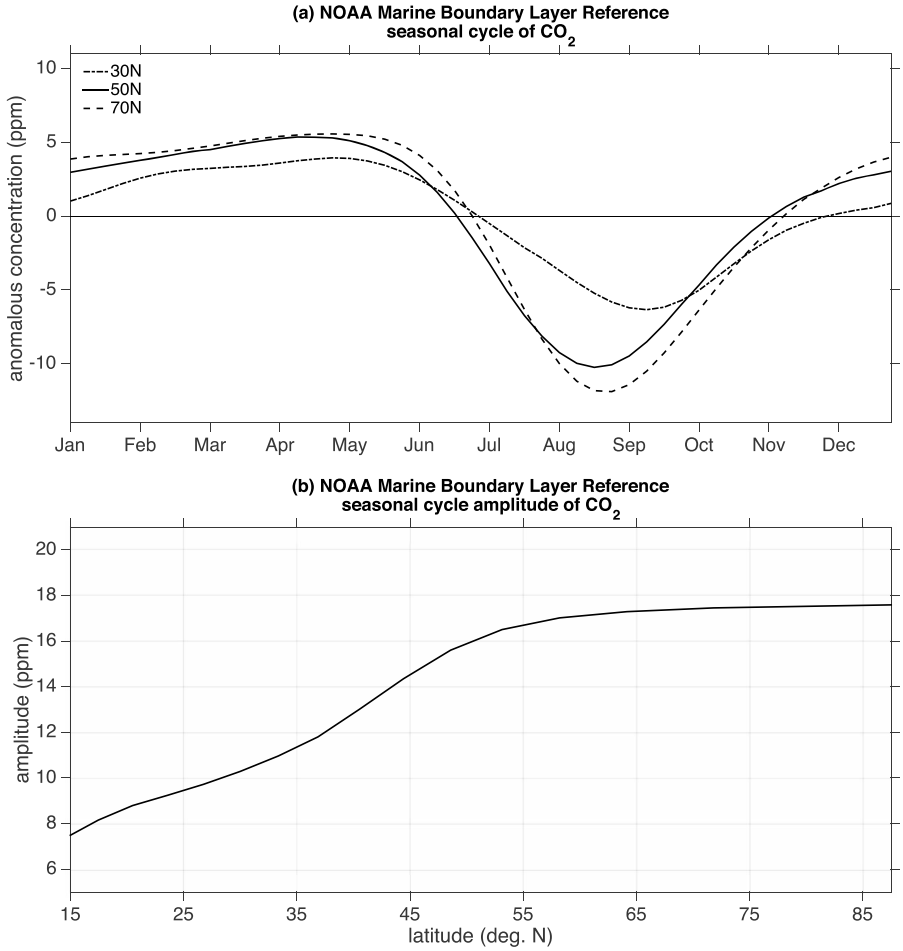

Figure 1. NOAA Marine Boundary Layer Reference 2009–2013 zonally averaged CO_2 (a) seasonal cycle and (b) seasonal cycle amplitude as a function of latitude.

of carbon metabolism on land [*Bacastow and Keeling*, 1981]. More recently, a number of studies have argued that the amplification of the seasonal cycle of CO_2 at high-latitude stations and from aircraft sampling reflects a response of northern ecosystems to climate change [*Graven et al.*, 2013; *Forkel et al.*, 2016] or to enhanced agricultural productivity [*Gray et al.*, 2014; *Zeng et al.*, 2014]. Models of changes in carbon cycling in boreal and Arctic ecosystems are especially divergent [*Fisher et al.*, 2014a], which has led to a strong research emphasis on detailed regional measurements of atmospheric carbon budgets [*Miller and Dinardo*, 2012].

Attribution of changes in SCA to ecological processes in specific regions requires quantitative treatment of atmospheric transport. The observed SCA increases almost monotonically with latitude (see Figure 1b), yet biological productivity has a maximum in the midlatitudes (roughly 30°N–60 °N). Regional CO_2 budgets based on drawdown or sources in the atmospheric boundary layer show substantial effects of meridional advection [*Bakwin et al.*, 2004; *Helliker et al.*, 2004]. Meridional CO_2 transport by synoptic weather disturbances is systematically correlated with ecosystem metabolism on land [*Parazoo et al.*, 2008; *Hurwitz et al.*, 2004] and is acknowledged to play a critical role in determining the seasonal cycle at high latitudes (roughly poleward of 60°N) [*Fung et al.*, 1983; *Parazoo et al.*, 2011]. Attempts to construct regional carbon budgets for high-latitude ecosystems using observations of atmospheric carbon tracers [*Chang et al.*, 2014; *Henderson et al.*, 2015; *Karion et al.*, 2015] require detailed specification of meridional advective fluxes through lateral boundary conditions. Much of this synoptic transport is along surfaces of constant potential temperatures ("isentropic transport"), but diabatic processes such as condensation and radiation can also be important in the troposphere [*Crawford et al.*, 2003; *Barth et al.*, 2007; *Miyazaki et al.*, 2008; *Pauluis et al.*, 2010]. Atmospheric transport by synoptic weather systems is systematically hidden by clouds from space-based observing systems and thus can lead to mischaracterization of seasonal cycles [*Corbin et al.*, 2009].

In this paper, we explore the fundamental relationships between surface carbon fluxes and atmospheric transport that can explain the seasonal cycle amplitude of CO_2 throughout the troposphere, paying particular attention to isentropic transport across latitudes. Our analysis includes both a widely used transport model derived from meteorological reanalysis and a much simpler moist aquaplanet that can also capture the relevant dynamics. We explore the effect of both surface fluxes and transport to isolate contributions of different latitudes and transport processes to the SCA of CO_2.

2. Data and Experimental Design

2.1. NOAA Marine Boundary Layer Reference

Figure 1 displays results from the National Oceanic and Atmospheric Administration (NOAA) Greenhouse Gas Marine Boundary Layer Reference data set [*Dlugokencky et al.*, 2015]. This data product is derived from weekly air samples from the NOAA Earth System Research Laboratory Carbon Cycle Cooperative Global Air Sampling Network and is smoothed in time and interpolated in space to produce a weekly zonally averaged data set of near-surface CO_2 as a function of time and latitude. To be consistent with the model simulations, we only analyze 2009–2013, although we have confirmed that using the entire record of 1979–2014 produces similar results.

2.2. GEOS-Chem

GEOS-Chem is a global 3-D chemical transport model for atmospheric composition that uses GEOS (Goddard Earth Observing System) assimilated meteorological fields from the NASA Global Modeling and Assimilation Office to simulate global atmospheric composition, including CO_2 [*Bey et al.*, 2001]. Dynamics include horizontal and vertical advection, turbulent diffusion, and moist convection. We use the CO_2 mode which ignores chemistry but contains atmospheric CO_2 fields. GEOS-Chem has been used extensively in studies of atmospheric CO_2 and quantitative attribution of surface carbon fluxes and compares well against a range of surface, airborne, and satellite CO_2 observations [e.g., *Parazoo et al.*, 2013; *Wunch et al.*, 2013; *Messerschmidt et al.*, 2013; *Nassar et al.*, 2010].

2.3. Land Surface Fluxes

Monthly biological CO_2 flux is simulated using the Community Land Model version 4.5 (CLM) [*Oleson et al.*, 2013] using an experimental setup as described in *Le Quéré et al.* [2015]. CLM is forced by time-varying reanalysis meteorology taken from the combined Climatic Research Unit and National Center for Environmental Prediction data set, which merges high-frequency variability from the National Centers for Envornmental Prediction-National Center for Atmospheric Research analysis [*Kalnay et al.*, 1996] with the monthly mean climatologies from the Climatic Research Unit (CRU) temperature and precipitation data sets [*Harris et al.*, 2014]. Monthly fossil fuel emissions are taken from Open-source Data Inventory of Anthropogenic CO_2 (ODIAC) [*Oda and Maksyutov*, 2011] and averaged over 2009–2013 to isolate the sensitivity of atmospheric CO_2 fields to seasonal biosphere exchange. We use GEOS-Chem version v9-01-01 with GEOS-5 fields on a $2° \times 2.5°$ grid (latitude $\times$ longitude) with 47 vertical layers. Simulations are spun up from 2000 to 2008 to establish hemispheric gradients. The experiments based on GEOS-Chem and CLM are described in more detail in *Parazoo et al.* [2016]. As we will demonstrate, the modeled CO_2 seasonal cycle from our GEOS-Chem/CLM setup compares well with that from the NOAA Marine Boundary Layer Reference data set.

Figure 2 depicts the zonally integrated CO_2 fluxes from the land surface to the atmosphere as a function of latitude and month averaged over the 2009–2013 period from CLM and ODIAC. On average, the land is a net source of CO_2 to the atmosphere (6.54 Pg C yr^{-1}), contributing 9.21 Pg C yr^{-1} from fossil fuels and removing 2.67 Pg C yr^{-1} from the atmosphere through biosphere uptake. However, biosphere fluxes are strongly seasonal. In the winter, the biosphere is a net CO_2 source driven by soil respiration, as denoted by the positive fluxes (warm colors). In the summer, the biosphere is a net CO_2 sink driven by photosynthesis, as denoted by the negative fluxes (cool colors). Fossil fuel emissions are positive all year, leading to a slightly enhanced winter source and reduced summer sink.

We note that GEOS-Chem simulations also include a CO_2 flux term that accounts for air-sea exchange over the oceans [*Takahashi et al.*, 2009], which removes an additional 1.43 Pg C yr^{-1} from the atmosphere, reducing total source emissions to 5.11 Pg C yr^{-1}. Although absorption by the ocean reduces the rate of increase of atmospheric CO_2 concentration, our analysis removes all long-term trends. Furthermore, ocean uptake does not have strong seasonality compared to land fluxes. The ocean is therefore not expected to impact our interpretation of the climatological seasonal cycle, and as discussed below is not included in simulations with the

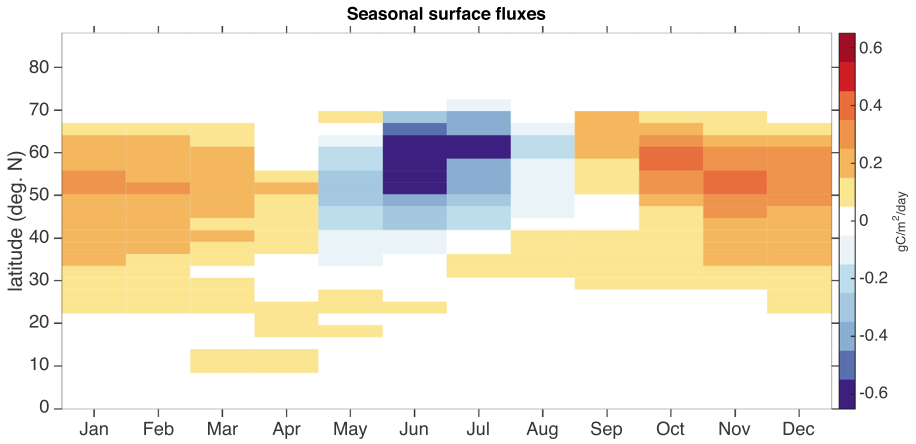

Figure 2. Annual average seasonal cycle of the surface fluxes of CO_2 as a function of latitude for 2009–2013 as simulated by CLM.

idealized general circulation model (GCM). We finally note that simplifications have been made when coupling CLM to GEOS-Chem, for example, not including the diurnal cycle of the fluxes. However, the purpose of this study is to explore fundamental dynamical transport mechanisms, and as we will show, the relevant transport pathways are well captured by the GEOS-Chem and idealized model simulations.

2.4. Idealized GCM

We use the gray-radiation aquaplanet general circulation model (GCM) described in *Frierson et al.* [2006]. The model physics includes gray radiative transfer such that water vapor has no effect on the radiative fluxes but can still influence the climate through latent heating and cooling. There are no clouds in this model, and radiative fluxes are a function of temperature only. The surface is a slab mixed layer ocean that is zonally symmetric (i.e., no topography). As in *Frierson et al.* [2006], we run the model without a convective parameterization using large-scale condensation only. All parameters are defined as in *Frierson et al.* [2006] except that their model configuration did not include a seasonal cycle. Thus, we simulate a seasonal cycle by varying the insolation as a function of the day of the year, using a 360 day calendar. Details of this procedure are provided in the appendix. The model is run at a horizontal resolution of T42 with 25 vertical levels and a time step of 900 s. The model does not simulate a realistic stratospheric circulation, which is intentional on our part, as we wish to focus exclusively on the tropospheric transport component of the SCA of the idealized tracers.

The aim of this study is to explore the fundamental relationship between the seasonal surface carbon fluxes and the tropospheric transport pathways that drive the seasonal cycle amplitude of CO_2 throughout the troposphere. The idealized model is an excellent tool for studying these basic transport mechanisms as it isolates the fundamental dynamics by removing many of the additional complexities of the real world. As we will show, even with these simplifications, the idealized model captures the observed seasonal behavior of CO_2 and thus is used to study the mechanisms responsible.

2.5. Tracer Setup

An idealized tracer is added to the gray aquaplanet, with surface sources and sinks driven by the monthly surface fluxes depicted in Figure 2. Specifically, the sources and sinks of the tracer are confined to the bottom layer of the model, are zonally symmetric, and are added (or subtracted) to each air parcel that enters the bottom boundary. The model integrates the tracer in units of mixing ratio, and so, the fluxes were converted into a mixing ratio per time step before being input into the model. Note that converting from a flux to a mixing ratio requires calculating the mass of air in the bottom model layer. Since our model has no topography, we have confirmed that the results are for all purposes identical if one assumes a constant mass of the bottom layer of the model, which is done here for simplicity. The idealized tracer is initialized at the start of the simulation and is integrated using a Lin-Rood semi-Lagrangian scheme [*Lin and Rood*, 1996] for horizontal advection and a finite-volume parabolic scheme for the vertical advection [*Lagenhorst*, 2005], with no explicit diffusion applied to the tracer. The model is integrated with a global "mass fixer" to ensure that the global tracer mass

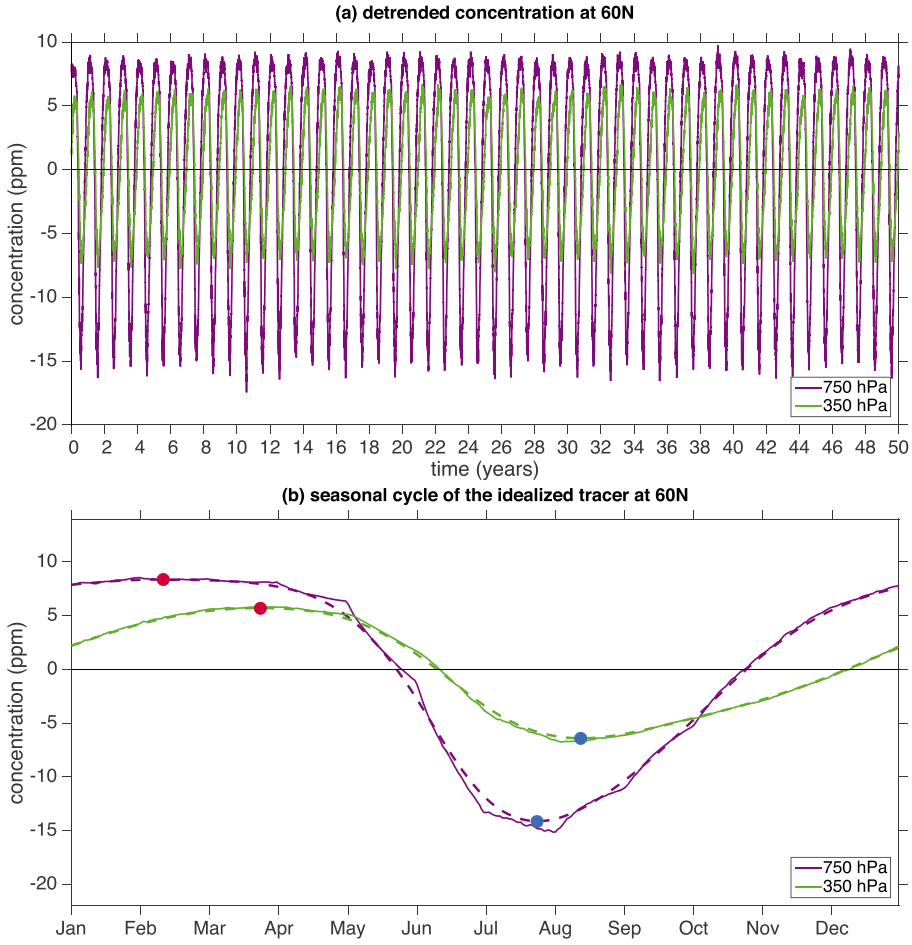

Figure 3. (a) The zonal mean concentration of the idealized tracer as a function of time at 60°N. (b) The climatological mean seasonal cycle of the idealized tracer at 60°N. The dashed line denotes the smoothed cycle (see text for details), and the circles denote the maximum (red) and minimum (blue) of the smoothed curves.

remains unchanged after every application of the advection operator (before the addition/removal by the surface source). This idealized tracer is identical to that used by *Orbe et al.* [2013] in a dry version of a similar idealized GCM but with different sources and sinks.

Integrating the fluxes in Figure 2 over an entire year yields a positive total flux driven by fossil fuel emissions. This drives a linear increase in the tracer with time. Our results are insensitive to this increase, and all of the subsequent analysis is performed on the detrended time series, as shown in Figure 3a for the zonally averaged tracer at 60°N for two different pressure levels. A seasonal cycle is evident in Figure 3a, with the seasonal cycle amplitude (peak to trough) being larger at 750 hPa (purple) compared to 350 hPa (green). The details of this seasonal cycle will be the focus of the analysis in the subsequent sections.

Our goal is to study the transport pathways that determine the overall structure of the SCA of CO_2 throughout the troposphere. Thus, to easily compare the structure of the SCA between the idealized model and GEOS-Chem simulations, rather than the actual magnitudes which differ due to the different model setups and assumptions, we scale all of the idealized tracer concentrations in the idealized simulations by a single value to easily compare them with those from GEOS-Chem. The scaling value used is the SCA at 50°N and 750 hPa in the GEOS-Chem Control simulation, so that the idealized model and GEOS-Chem have the same SCA at this location, and thus, their relative variations with latitude can be easily compared. We note that our conclusions do not change if a different location is used to define the scaling.

2.6. Experiments

Five experiments were explored with the idealized aquaplanet. Each experiment is composed of 54 year simulations with the first 4 years discarded for spin-up leaving 50 years for analysis. A summary of each experiment

Table 1. Idealized Aquaplanet Tracer Experiments

Name	Description
Control	The atmosphere exhibits a seasonal cycle and the idealized tracer sources and sinks are as shown in Figure 2.
Equinox	As in Control, except the atmosphere is held at Equinox conditions (i.e., no seasonal cycle) while the seasonality of the fluxes is maintained.
ArcticOff	As in Control, except the fluxes at and poleward of 60°N are set to zero.
AddMaxMin 30°N	As in Control, except the tracer fluxes are perturbed by 0.05 gC/m^2/dy in the months of their maximum and minimum fluxes at 30°N.
AddMaxMin 40°N	As in AddMaxMin 30°N except for fluxes at 40°N.
AddMaxMin 50°N	As in AddMaxMin 30°N except for fluxes at 50°N.
AddMaxMin 60°N	As in AddMaxMin 30°N except for fluxes at 60°N.
AddMaxMin 70°N	As in AddMaxMin 30°N except for fluxes at 70°N.

is given in Table 1 with the details described in the following subsections. All simulations but the Equinox simulation have identical circulations at all time steps since we initialized all simulations in the same way. Thus, the atmospheric flow field evolves in exactly the same way with only the passive tracer concentrations differing across simulations. This is not the case for the Equinox simulation, as the circulation is modified by the lack of a seasonal cycle (to be discussed).

2.6.1. Control

The Control simulation has a seasonal cycle in the atmosphere, determined by the dynamic and thermodynamic response to changes in insolation. The monthly tracer sources and sinks are as defined in Figure 2.

2.6.2. Equinox

The Equinox simulation removes the seasonal cycle of the circulation by setting the insolation equal to its equinoctial value. However, in this simulation, the tracer surface fluxes still evolve seasonally as in Figure 2. Thus, the seasonality of the atmospheric circulation is removed, while the seasonality of the fluxes is maintained. This setup allows us to quantify the role of the seasonality of the circulation in driving seasonality in the idealized tracer.

2.6.3. ArcticOff

The ArcticOff simulation is identical to the Control except the Arctic fluxes (i.e., both sources and sinks) at 60°N and poleward are set to zero. This simulation is designed to quantify the role of Arctic surface fluxes in driving the tracer seasonal cycle throughout the troposphere.

2.6.4. AddMaxMin

One point of interest here is how a small change in the tracer source and sink at one latitude can impact the SCA of the tracer at another latitude and altitude. Thus, the AddMaxMin experimental setup is simulated 5 times—once for a perturbation at each of the following five latitudes: 30°N, 40°N, 50°N, 60°N, and 70°N. Specifically, we increase the surface flux at the relevant latitude by 0.05 gC/m^2/d in the month of maximum source and decrease the surface flux at each latitude by 0.05 gC/m^2/d in the month of maximum sink (i.e., the month of minimum fluxes). Thus, while there is no net increase in annual tracer flux, this perturbation introduces a small enhancement of the preexisting seasonal cycle of the tracer emissions. This process is depicted in Figure 4, where we plot the seasonal cycle of surface fluxes at each of the five latitudes, and the filled circles denote the months of maximum and minimum fluxes. Note the *y* axis, which ranges from −1.0 to 0.5 gC/m^2/d, highlighting that a perturbation of ±0.05 gC/m^2/d is small. This experiment results in five different simulations and will be used to discuss the relative importance of changes in the seasonal cycle of emissions at different latitudes in driving changes in the SCA throughout the troposphere.

We note that one could instead perturb the fluxes during the same 2 months (rather than at the seasonal cycle extrema) for each simulation. However, given the different phasing of the seasonal cycle at the different latitudes (Figure 4), this can result in an attenuation or even a reversal of the seasonal cycle for some latitudes while amplifying the seasonal cycle at other latitudes. Furthermore, recently observed changes in the SCA of CO_2 take the form of an amplification of the present-day seasonal cycle [e.g., *Graven et al.*, 2013, Figure 2], and thus perturbing the fluxes at their seasonal maximum and minima is most relevant to this study.

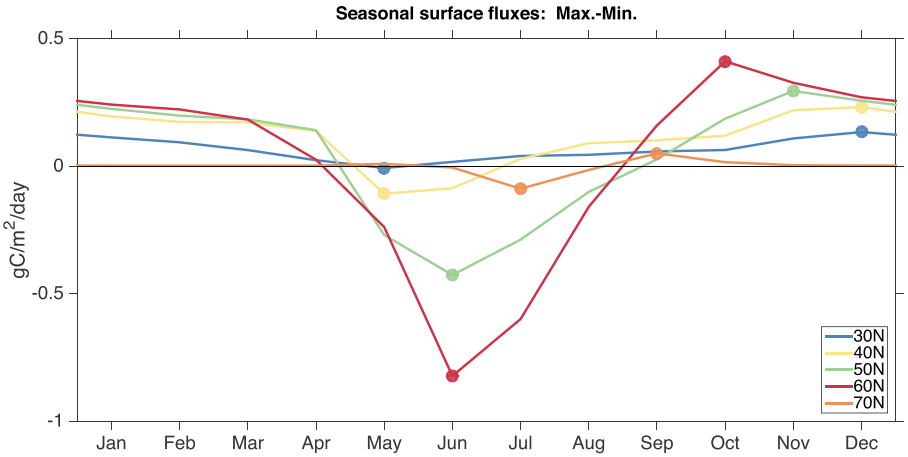

Figure 4. Surface fluxes of the idealized tracer showing the maximum and minimum months. See text for additional details.

Finally, we note that *Keppel-Aleks et al.* [2011] performed similar experiments to explore the response of the total-column SCA to perturbations of surface fluxes at different latitudes except that they scaled each latitude's perturbation so that the Northern Hemisphere net primary production increased by 25% in every case. We have intentionally used a fixed flux perturbation (i.e., ± 0.05 gC/m^2/d) to test how the SCA may respond if each meter squared of biosphere underwent the same physical change at each of the five latitudes.

2.7. Calculation of the Seasonal Cycle Amplitude (SCA)

It is evident from Figure 3a that the tracer exhibits a strong seasonal cycle and that the seasonal cycle amplitude varies throughout the troposphere. We quantify the SCA by calculating the smoothed climatological seasonal cycle of the zonally averaged tracer concentrations at every pressure level and latitude. Figure 3b shows an example of this seasonal cycle at 60°N for the lower troposphere (750 hPa; purple) and the upper troposphere (350 hPa; green). The solid lines in Figure 3b denote the raw curves, and the dashed lines denote the curves smoothed with a moving average window of length 31 days applied forward and backward. The red and blue dots denote the maximum and minimum concentrations, respectively, over the smoothed seasonal cycle at each point, and the SCA is defined as the difference between these extrema.

3. Results

3.1. Control Simulation

The 50 year mean anomalous March tracer concentrations, defined as the deviation from the 50 year annual mean, are shown in Figure 5a for the Control simulation of the idealized aquaplanet. March is chosen because late winter/early spring is when the tracer concentrations are largest throughout the troposphere, consistent with the timing of when the winter time source has had time to build up tropospheric concentrations, but the surface sink has not yet appeared (see Figure 2). The March circulation is also representative of the cool season circulation when poleward isentropic transport by the storm tracks is strongest. The concentrations are largest near the surface, peaking slightly poleward of the maximum surface source during this month (red rectangles), and decrease as one moves away from the surface. Lines of constant potential temperature (isentropes) are plotted as thick black lines. It is evident that the tracer concentrations roughly follow these isentropic surfaces, sloping upward and poleward, which is expected since isentropic transport by the winter time midlatitude storm track is known to be an important pathway for the poleward transport of CO_2 [*Miyazaki et al.*, 2008; *Parazoo et al.*, 2011; *Keppel-Aleks et al.*, 2012] and other atmospheric constituents [e.g., *Klonecki et al.*, 2003; *Stohl*, 2006]. We do note, however, that the concentrations do not align exactly with the dry isentropes due to cross-isentropic transport induced by, for example, diabatic heating within the midlatitude storm tracks [e.g., *Klonecki et al.*, 2003; *Parazoo et al.*, 2011]. To support the use of such an idealized model in properly simulating the transport of CO_2, Figure 5b shows the same anomalous March CO_2 concentrations from GEOS-Chem. While small differences can certainly be found, the general observation that the CO_2 concentrations peak near the surface just poleward of the maximum source and that the CO_2 concentrations slope upward and poleward are clearly evident in both models.

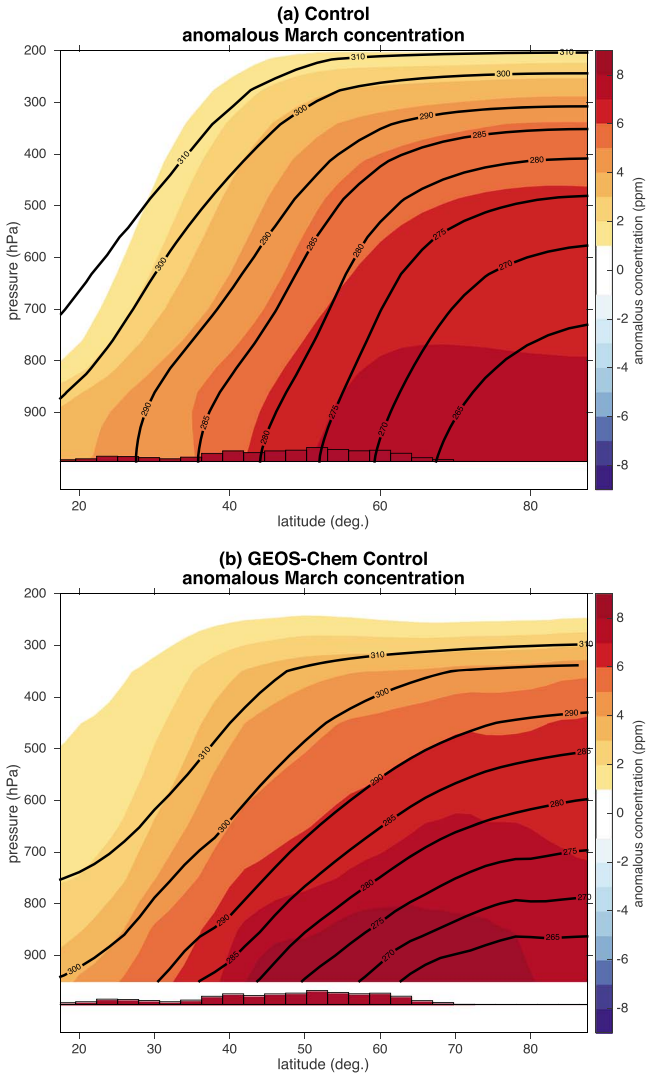

Figure 5. The anomalous March concentration of (a) the tracer in the idealized model and (b) CO_2 in GEOS-Chem. Black lines denote the March isentropes. Rectangles at the lowest level represent the March source at that latitude.

Our interest here is the seasonality of tracer concentrations, and so Figure 6a shows the smoothed climatological seasonal cycle of the idealized tracer at 750 hPa in three different latitude bands: the subtropics (30°N), the midlatitudes (50°N), and the Arctic (70°N). In a broad sense, the concentration of the tracer at each of the three locations follows a similar seasonal progression, peaking in the late winter/early spring and reaching a minimum in late summer. However, closer inspection reveals that the amplitude of the seasonal cycle is smallest for the most equatorward location (30°N; dotted line) and largest for the most poleward location (70°N; dashed line), with the summer minimum occurring later in the season for 30°N. Such behavior is also seen in the observations (compare Figure 6a and Figure 1a), providing confidence in the model's ability to capture the relevant aspects of the seasonal cycle of CO_2. To explore this further, we compute the SCA at each latitude band at four different pressure levels in the idealized model and plot the SCA in Figure 6b as a function of latitude. The dashed gray line denotes the seasonal cycle amplitude of the surface fluxes (Figure 2). Although the seasonal amplitude of the surface fluxes peaks near 55°N and is close to zero at higher latitudes, the SCA of the tracer throughout the troposphere increases monotonically as one moves to higher and higher latitudes (Figure 6b; 750 hPa, 550 hPa, and 350 hPa). Near the surface at 850 hPa, and thus near the tracer source and sink, the SCA increases with latitude until around 65°N, where it begins to decrease slightly (as will be discussed, this decrease at high latitudes is also seen at 850 hPa in GEOS-Chem; Figure 10b). As discussed in section 1, this general increase in SCA with latitude throughout the troposphere is a well-known aspect of

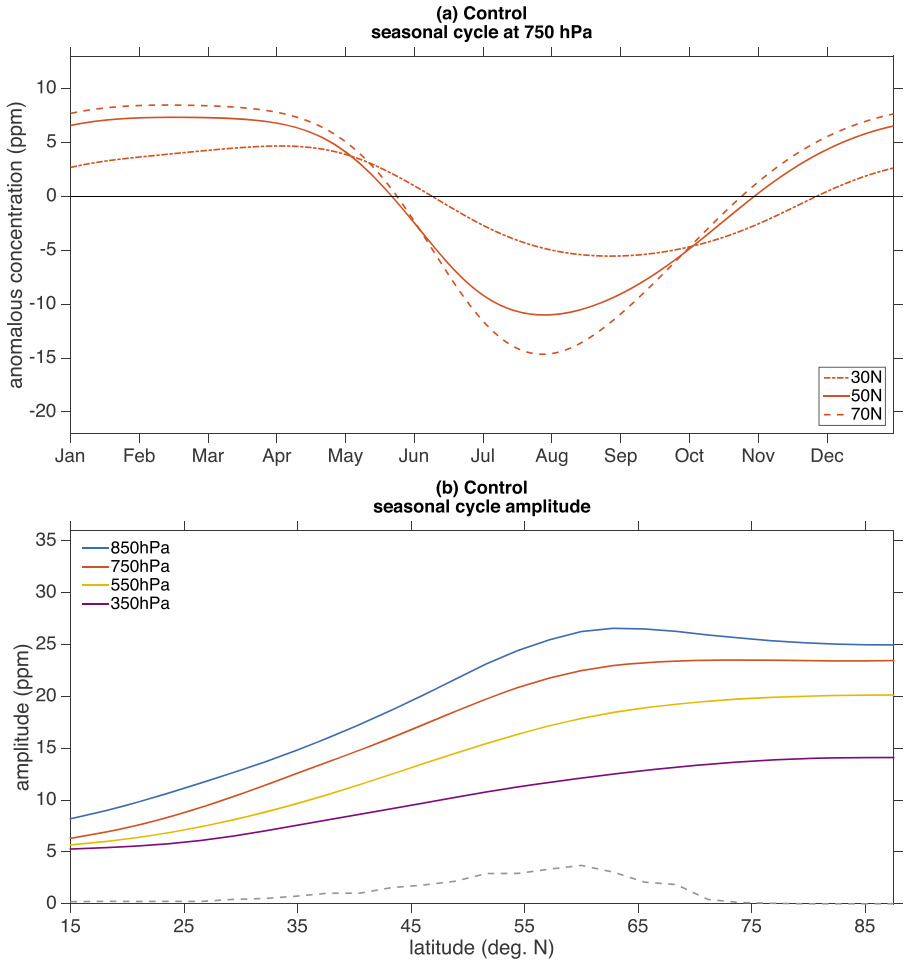

Figure 6. (a) The seasonal cycle of the idealized tracer at 750 hPa and (b) the seasonal cycle amplitude as a function of latitude in the Control simulation. The dashed gray line in Figure 6b denotes the seasonal amplitude of the surface fluxes scaled to arbitrary units for visualization purposes only.

observed CO_2 concentrations (compare to Figure 1b) and is in stark contrast to the seasonal amplitude of the surface emissions which peak in midlatitudes. Thus, even though the model is an idealized aquaplanet, e.g., no clouds, no topography, no dynamic biosphere, the seasonal cycle amplitude of the idealized CO_2 tracer increases with latitude as it does in the observations (Figure 1b) and in GEOS-Chem (to be discussed). We will use these idealized simulations to explore why this might be the case.

3.2. Isentropic Transport and the SCA

Figure 6b demonstrates that the SCA generally increases with latitude along four different pressure surfaces. It is thus informative to visualize the SCA at all points throughout the troposphere, and this is shown in Figure 7a, where the colors denote the SCA at each latitude and altitude. Note that horizontal cross sections of Figure 7a produce the curves shown in Figure 6b. As was the case for the concentrations (Figure 5), the SCA is largest near the surface and decreases upward for a fixed latitude (as we also saw in Figure 3b at 60°N). But, more importantly, contours of SCA do not lie horizontally along pressure surfaces but rather curve upward and poleward. Thus, not only is the tracer being transported along isentropes but also is the seasonality.

As an example, consider the surface fluxes near 30°N. These fluxes drive a particular seasonality in the tracer concentrations there. This seasonality is transported along the 290 K isentrope and thus is transported to the upper troposphere (350 hPa) by the time it reaches Arctic latitudes. This can be seen more clearly in Figure 8a, where we plot the smoothed climatological seasonal cycle of the tracer along the 290 K isentrope, rather than along a pressure surface. From this viewpoint, the seasonal cycle and its amplitude are nearly identical across all three latitudes. Furthermore, plotting the 290 K SCA in Figure 8b (blue line) shows that the SCA no

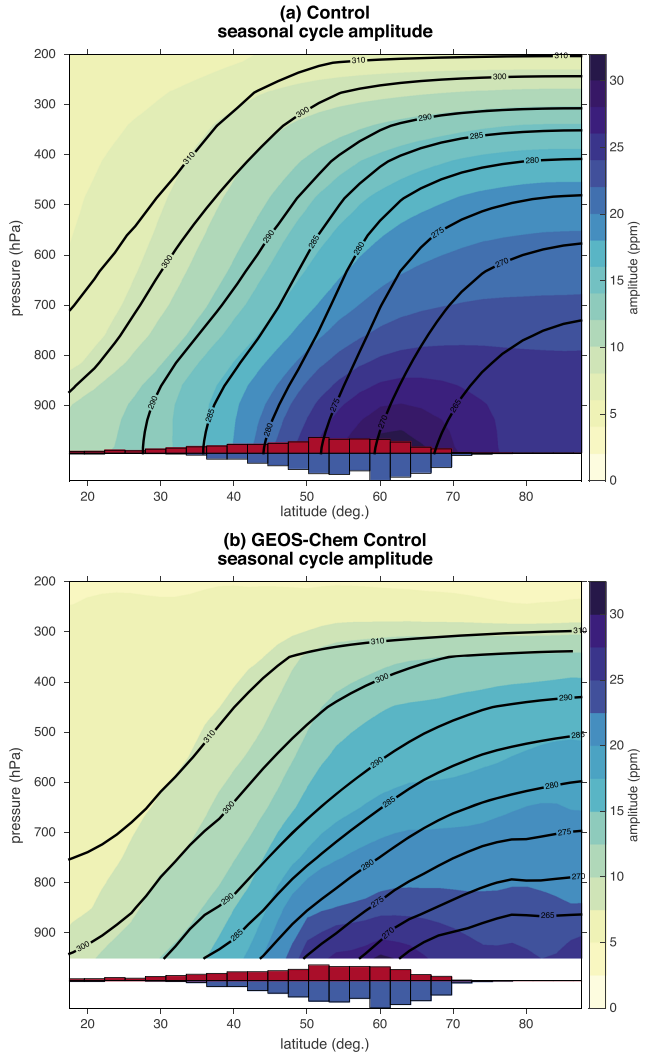

Figure 7. Seasonal cycle amplitude of (a) the tracer in the idealized model and (b) CO_2 in GEOS-Chem. Black lines denote the March isentropes. Rectangles at the lowest level represent the average source (red) and sink (blue) throughout the year at that latitude.

longer increases with latitude but rather is nearly constant as expected from Figure 7. The 285 K isentrope (red) also exhibits nearly constant SCAs of the tracer for all latitudes. The constant SCA with latitude begins to breakdown for the tracer along the 280 K isentrope (yellow) as this isentropic surface is located in the lower troposphere at high latitudes where cross-isentropic sinking of the tracer (and its seasonality) due to radiative cooling becomes important [e.g., *Klonecki et al.*, 2003; *Miyazaki et al.*, 2008].

The fact that the tracer, and thus its seasonality, is transported to high latitudes along isentropic surfaces can account for why the SCA of the tracer increases with latitude along pressure surfaces. Due to the upward and poleward transport of CO_2 along isentropic surfaces, the SCA in the high latitudes is a reflection of the tracer's surface fluxes farther equatorward. Thus, even though the surface fluxes near the pole are zero, the largest SCAs are found in the high-latitude troposphere since they correspond to isentropes that intersect the midlatitude surface in the vicinity of the maximum surface flux seasonality (e.g., 55°N).

For further support, Figure 7b shows the SCA of CO_2 from GEOS-Chem. While our idealized model has no continents or topography and fully determines its own dynamics, GEOS-Chem advects CO_2 according to reanalysis winds and thus includes all of the complexity of the real-world circulation. Comparing the SCAs from the idealized aquaplanet with the GEOS-Chem reveals very similar behavior of the seasonal cycle amplitude, with the SCA sloping up and poleward along isentropic surfaces. GEOS-Chem does exhibit stronger diabatic

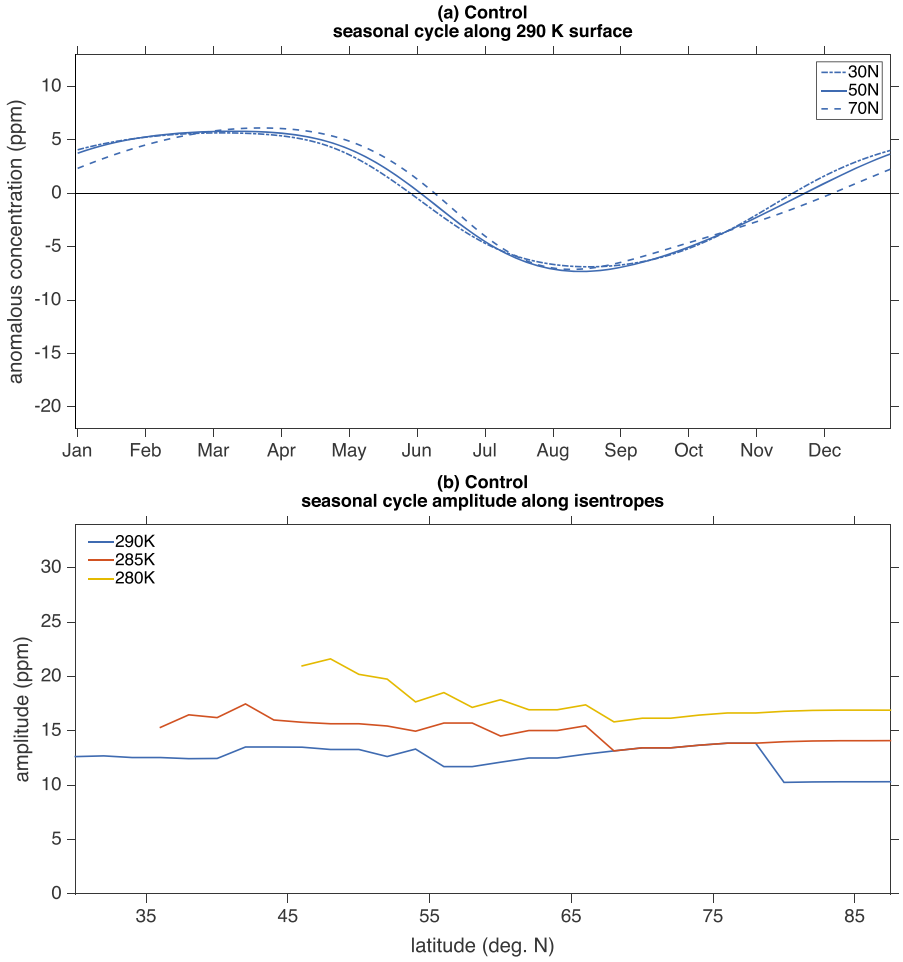

Figure 8. (a) The seasonal cycle of the idealized tracer along the 290 K isentropic surface and (b) the seasonal cycle amplitude along isentropic surfaces in the Control simulation. Isentropic surfaces are defined along their March climatological location (see text for details).

subsidence at high latitudes compared to the idealized model, likely due to the larger radiative cooling associated with extremely cold temperatures over land in winter. Along with the more horizontal isentropes in GEOS-Chem compared to the idealized model, it is likely that the SCA of CO_2 in high latitudes is even more influenced by lower latitude fluxes in GEOS-Chem. That is, the surface fluxes at 30°N are transported to 450 hPa over the Arctic in GEOS-Chem, rather than 350 hPa in the aquaplanet. The overall agreement between the idealized model and GEOS-Chem, however, provides strong evidence that the surface fluxes in the Arctic region (e.g., poleward of 60°N) are not required for the SCA to increase with latitude along pressure surfaces. We will further test this hypothesis in the following section.

3.3. Arctic Versus Midlatitude Drivers

We next quantify the role of the Arctic surface fluxes in driving the seasonal cycle of the tracer throughout the high latitudes. We will demonstrate that while these fluxes certainly play a role, it is the midlatitude surface fluxes that drive the majority of the high-latitude seasonal cycle all throughout the troposphere.

To quantify the importance of Arctic surface fluxes, we ran an additional simulation, termed ArcticOff, where the Arctic surface fluxes (both sources and sinks) were set to zero. Figure 9a shows the SCA of the idealized tracer in this simulation. The SCA is smaller in the ArcticOff simulation compared to the Control (Figure 7a), as one might expect due to the absence of Arctic surface fluxes. However, the main point is that the structure of the SCA is the same between the Control and ArcticOff simulations, with lines of constant amplitude roughly following isentropic surfaces. It is evident that taking an isobaric slice (along a pressure surface) of Figure 9 will lead to increasing SCA with latitude, and these profiles are shown in Figure 10a as dashed lines

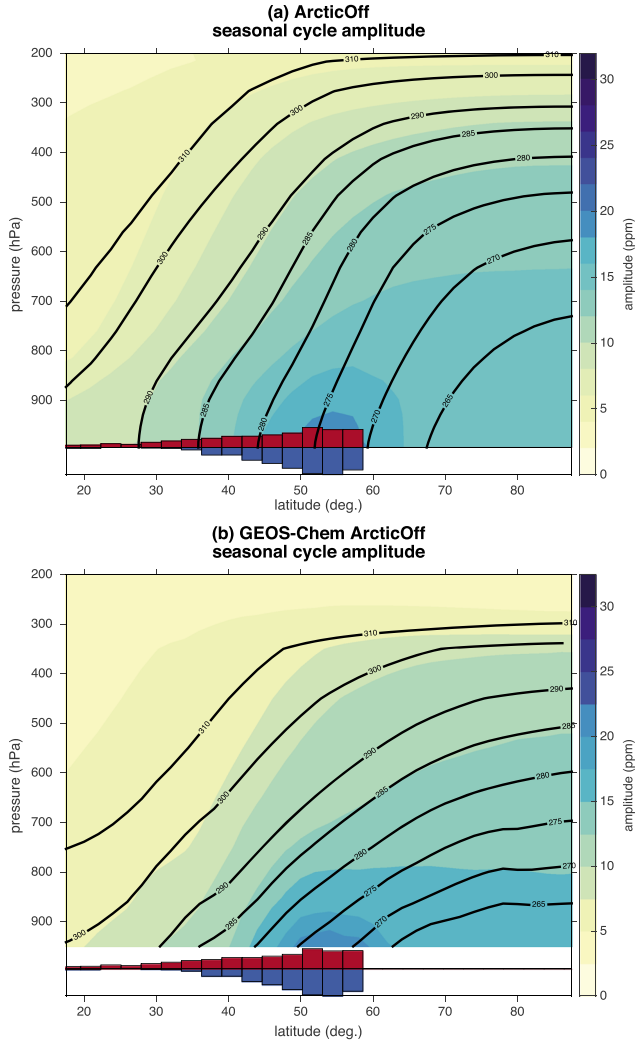

Figure 9. Seasonal cycle amplitude of (a) the tracer in the idealized model and (b) CO_2 in GEOS-Chem in the ArcticOff simulations where Arctic surface fluxes are turned off. Black lines denote the March isentropes. Rectangles at the lowest level represent the average source (red) and sink (blue) throughout the year at that latitude.

(the Control is shown in solid lines for comparison). For the ArcticOff simulation, the SCA increases with latitude for all four pressure surfaces, except 850 hPa where it levels off around 55°N. Thus, a main finding is that the increase in SCA with latitude does not require Arctic surface fluxes at all. Comparing the ArcticOff SCAs (dashed lines) with those from the Control (solid lines) in Figure 10a, we find that the Arctic surface fluxes account for less than 40% of the SCA above 900 hPa at all latitudes.

To provide further support, we have performed the same ArcticOff simulation with GEOS-Chem. Figures 9b and 10b show the SCA from GEOS-Chem as done for the idealized aquaplanet. The results are very similar and also show that Arctic surface fluxes account for less than 35% of the SCA away from the surface when CO_2 is advected by the reanalysis winds in GEOS-Chem. The similarities in structure between the SCA in the idealized aquaplanet and GEOS-Chem further suggest that the idealized framework is capable of capturing the relevant transport.

While our previous findings demonstrate that the majority of the SCA at high latitudes is driven by surface fluxes at lower latitudes, they do not reveal the relative importance of changes in the fluxes at the midlatitude surface versus changes in the fluxes at the high-latitude surface. Thus, we perform an additional set of simulations, AddMaxMin, where we increase the magnitude of the surface fluxes (both the source and sink) at a single latitude to simulate a trend in the seasonal cycle amplitude of the surface fluxes without changing the net annual surface flux. Specifically, we enhance the seasonal cycle of emissions at 30°N–70°N by perturbing

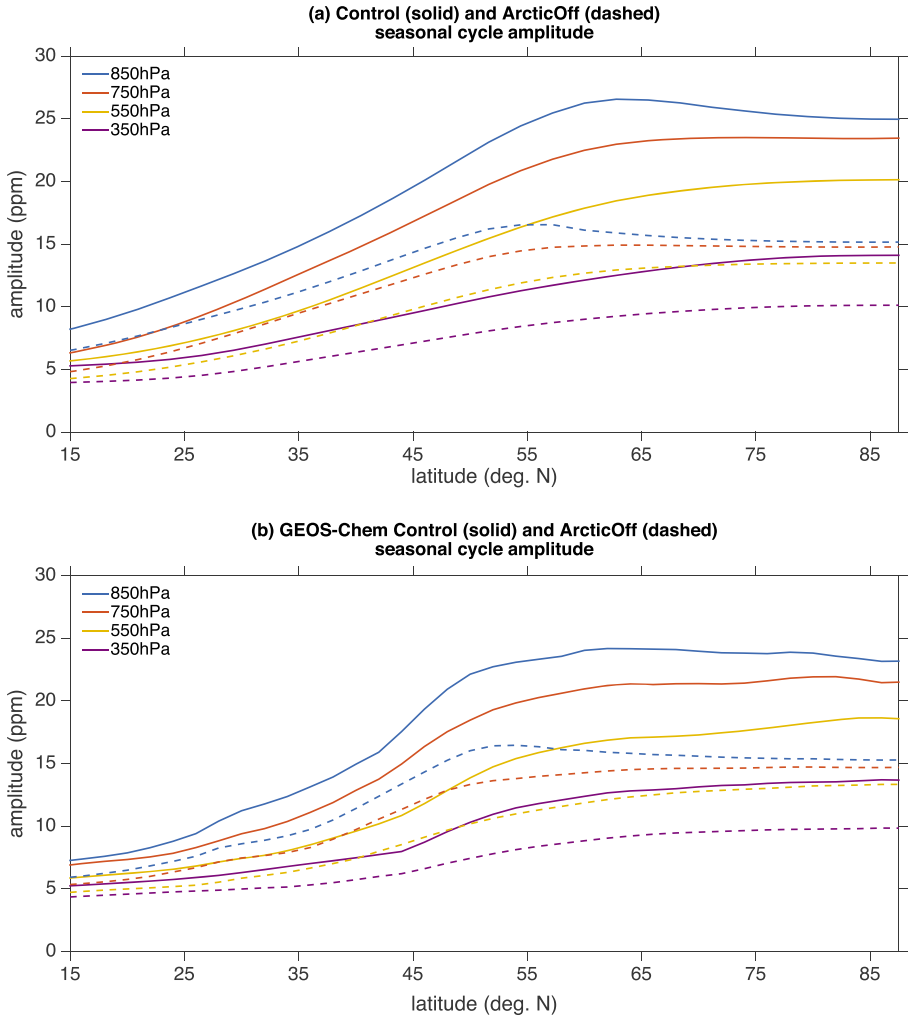

Figure 10. Comparison of the seasonal cycle amplitude of (a) the tracer in the idealized model and (b) CO_2 in GEOS-Chem for the Control and ArcticOff simulations.

the fluxes by a fixed amount (specifically, ± 0.05 gC/m^2/d) in the months with the maximum and minimum fluxes (as depicted in Figure 4). Note that the flux perturbations are not defined as a fractional change but rather are constant across simulations, in order to test each latitude consistently.

The resulting changes in the SCA at 350 hPa, 550 hPa, and 850 hPa are plotted in Figure 11. The five colored lines correspond to the amplitude change for the five different simulations where the fluxes at five different latitudes (colored rectangles) were perturbed. SCA changes for all perturbations at all latitudes are positive in Figure 11 indicating that increasing the seasonal cycle of the emissions increases the SCA of the tracer everywhere. However, the differences between the five simulations indicate that changes in the surface emissions at some latitudes are more important than changes at other latitudes. Specifically, in the upper (350 hPa) and middle troposphere (550 hPa)(Figures 11a and 11b), emission changes at 30°N (blue) and 50°N (green) dominate the changes in SCA at most northern latitudes, including the Arctic. Even near the surface at 70°N (the latitude of Barrow, Alaska; Figure 11c), the tracer SCA is more sensitive to an increase in seasonal fluxes at 30°N (blue) than 60°N (red).

To quantify the relative importance of these perturbations throughout the entire troposphere, we plot in Figure 12 the latitude perturbation which results in the largest change in SCA. Perturbations at 30°N (blue) and 50°N (green) have the largest impact on the SCA at nearly all locations, with perturbations at 40°N (yellow) and 60°N (red) making prominent contributions at select locations. We caution that the dominance of flux changes at 50°N in the subtropical middle to upper troposphere should not be overinterpreted, as they

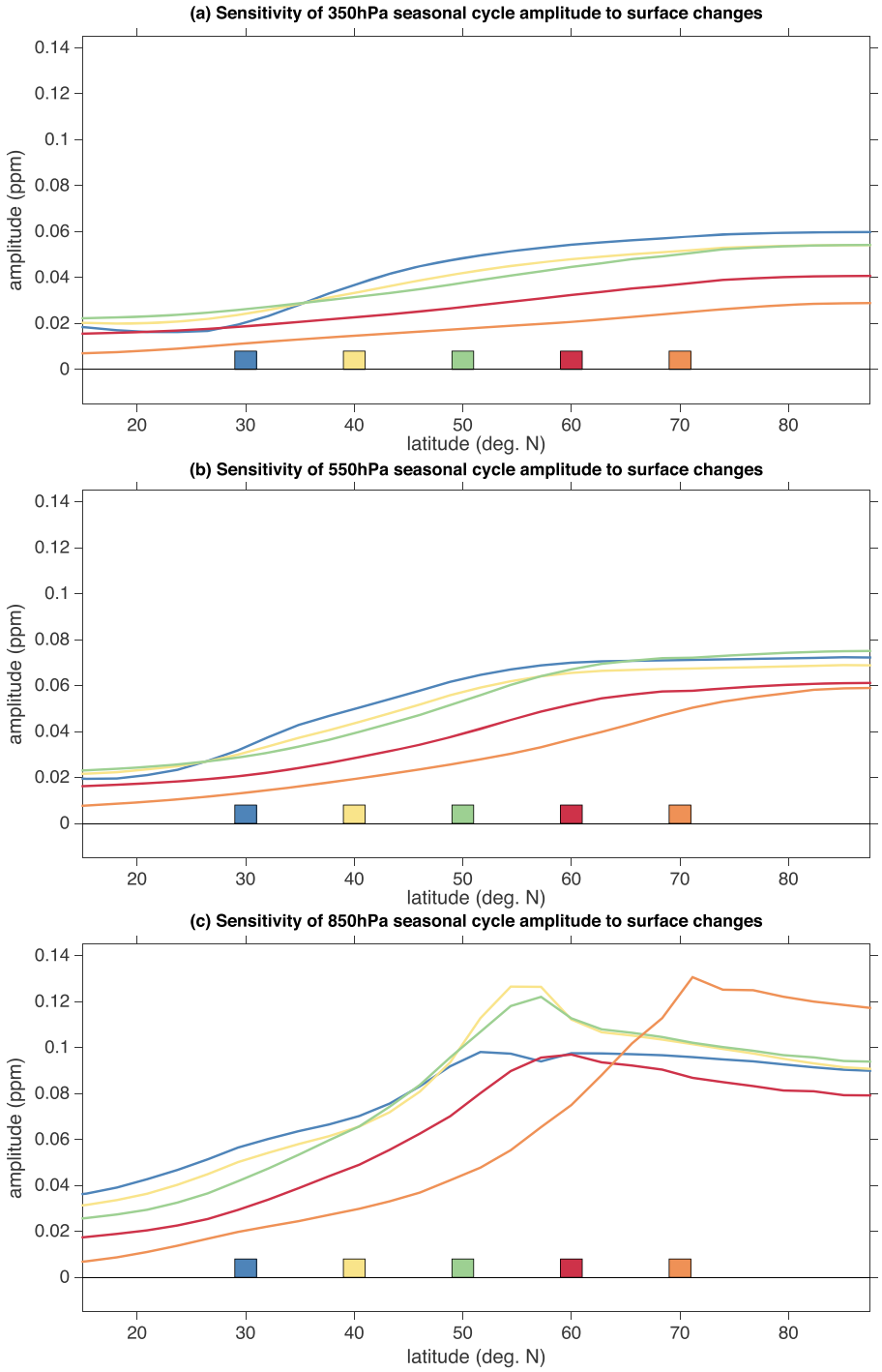

Figure 11. Change in the seasonal cycle amplitude driven by perturbations in the surface source/sink at individual latitudes (i.e., the AddMaxMin experiment) at different pressure levels. More positive values imply a larger SCA compared to the Control simulation and thus a larger influence by perturbations at that latitude. See text for additional details.

reflect only a marginally larger impact of 50°N compared to 30°N or 40°N (see Figures 11a and 11b). Changes in the surface fluxes at 70°N (orange) dominate the SCA near the Arctic surface but are not the most important contributor above 800 hPa. Put another way, a change in midlatitude surface fluxes will drive a larger response in the SCA than an equivalent change in Arctic surface fluxes at nearly all points in the troposphere. Finally, note that the influence of the 30°N perturbations (blue) slope poleward and upward, highlighting the role of isentropic transport in transporting these perturbations throughout the troposphere.

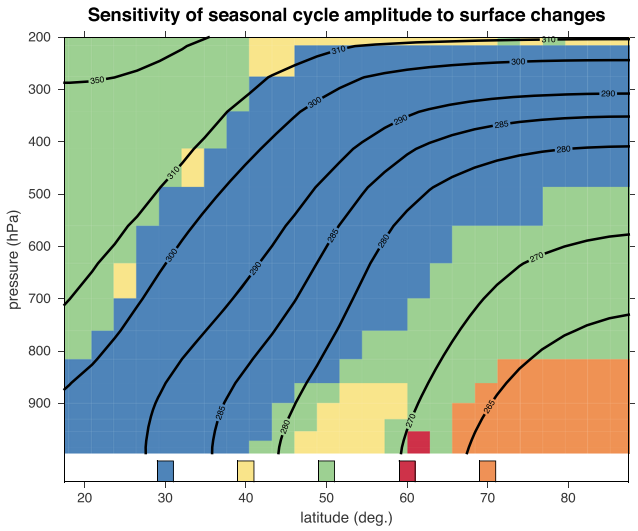

Figure 12. The latitude that most increases the seasonal cycle amplitude at each latitude/pressure point when the surface source/sink is perturbed in the months with the maximum and minimum source and sink, respectively. See text for additional details. Black lines denote the March isentropes.

The experimental design of the AddMaxMin simulations takes into account the larger area at lower latitudes compared to higher latitudes by defining the perturbation in terms of flux per meter squared. However, in the Northern Hemisphere, land is not distributed equally across latitude bands, but rather, the fraction of land at high latitudes is larger than the fraction at lower latitudes. Taking the fractional area that is land into account (using values *Hartmann* [1994, Figure 1-12]) leads to similar conclusions as found in Figure 12, except that contributions from 50°N dominate the tropospheric sensitivity, and the dominating influence of emissions changes at 70°N is felt at slightly higher altitudes (i.e., up to 650 hPa; not shown).

The results of this section can be summarized by two main conclusions. (1) The *majority* of the seasonal cycle amplitude of CO_2 at high latitudes is driven by fluxes outside of the Arctic (e.g., Figure 9 and Figure 10). (2) The seasonal cycle amplitude is most sensitive to changes in the seasonality of *midlatitude* surface emissions throughout most of the troposphere. Only near the Arctic surface are changes in emissions at the Arctic surface the dominant driver (e.g., Figure 12), although it contributes only 20% more than the flux changes at lower latitudes (Figure 11c) in the idealized model.

Drivers of the near-surface Arctic SCA are especially important since the majority of high-latitude CO_2 measurements are taken at or near the surface. Results from the idealized model suggest that near the surface, Arctic fluxes and midlatitude fluxes are both important contributors to the SCA there. We expect that if anything, the idealized model underestimates the influence of midlatitude fluxes on the SCA near the Arctic surface since the Arctic surface does not get cold enough in the idealized model, and thus, the diabatic cooling (and cross-isentropic sinking) is likely too weak. This sinking at high latitudes transports midlevel tracer (transported from lower latitudes) down, and thus, weaker sinking implies a weaker signature of lower latitude fluxes at the Arctic surface. Evidence of this can be seen in Figure 7, where the Arctic isentropes have steeper slopes in the idealized model compared to GEOS-Chem. Furthermore, comparing the ArcticOff experiments between the two models (Figure 10) shows that the idealized model suggests a smaller role for Arctic fluxes in driving near-surface SCA (35%; blue lines in Figure 10b) compared to the idealized model (40%; blue lines in Figure 10a).

3.4. Circulation-Driven Seasonality

Up until now, we have discussed the seasonality of the idealized tracer as a whole. However, this seasonality is actually driven by two separate components: (1) a seasonality in the tracer source/sink and (2) a seasonality in the atmospheric transport (i.e., circulation). In order to investigate the relative roles of each of these two components, we make use of our idealized modeling framework and discuss simulations where the seasonality of

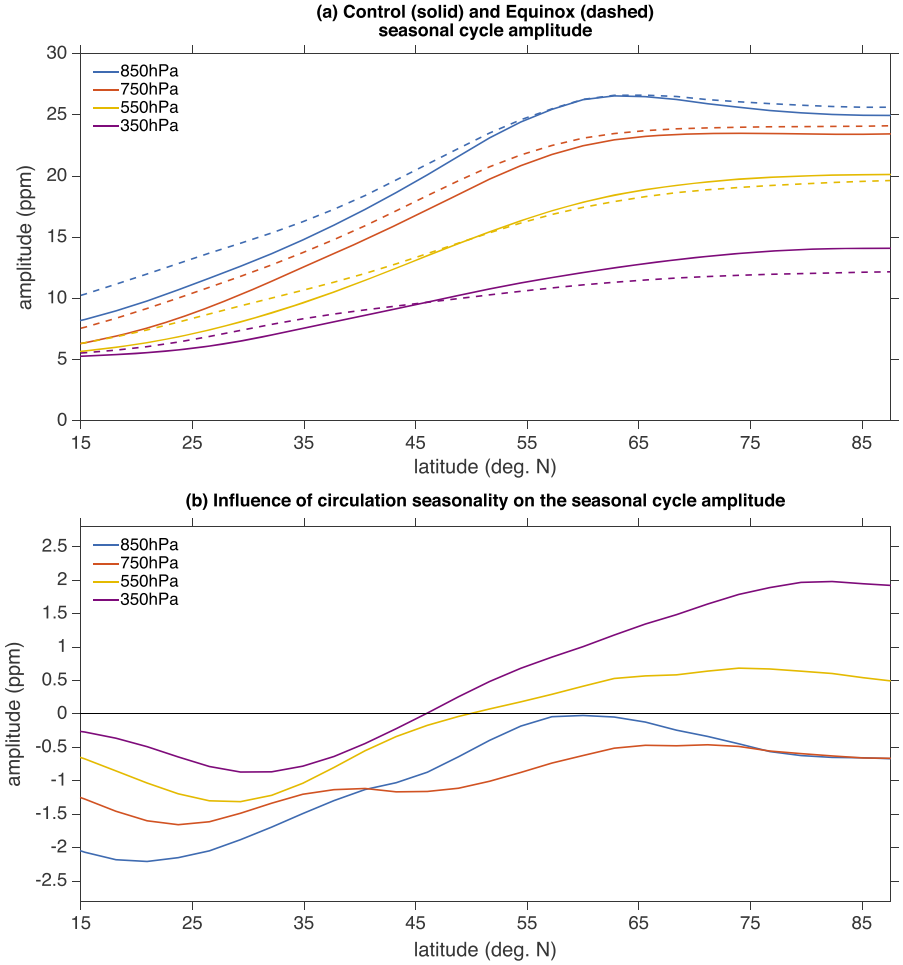

Figure 13. (a) Comparison of the seasonal cycle amplitude of the idealized tracer in the Control simulation and the Equinox simulation. (b) The difference between the Control simulation and the Equinox simulation seasonal cycle amplitudes, where positive values signify that the seasonality of the circulation enhances the seasonal cycle amplitude of the tracer there.

the circulation is removed (i.e., constant incoming solar radiation). We will show that although the seasonality of the surface fluxes dominates the total tracer seasonal cycle, the seasonality of the circulation contributes a nonnegligible amount.

To remove the influence of the circulation's seasonal cycle, we perform a simulation, termed Equinox, where the insolation is fixed to its equinoctial value for the entirety of the run but the tracer surface fluxes have the same seasonal cycle as the Control (i.e., Figure 2). Figure 13a shows the SCA as a function of latitude for the Equinox simulation (dashed lines) and the Control simulation (solid lines). The influence of the circulation's seasonal cycle on the tracer's SCA is inferred as the difference between the Control and the Equinox simulations, which is plotted in Figure 13b. Figure 13 suggests that while the circulation does not play a large role in determining the SCA, its influence is nontrivial. Specifically, in the lower troposphere (850 hPa and 750 hPa; blue and red lines) the circulation's seasonality acts against the surface flux seasonality to reduce the SCA (negative values in Figure 13b). However, in the middle and upper troposphere (550 hPa and 350 hPa; yellow and purple lines) the circulation's seasonality acts with the surface flux seasonality to increase the SCA poleward of 45°N (i.e., the latitude of the midlatitude eddy-driven jet). The differences in SCA between the Control and Equinox are on the order of 2 ppm, suggesting that the seasonality of the circulation can account for approximately 10–20% of the total SCA. We note that our results are consistent with *Parazoo et al.* [2011] who also found that the transient eddies (i.e., the storm tracks) act to enhance the seasonal cycle amplitude of column-integrated CO_2 at high latitudes.

4. Discussion and Conclusions

The results of this study can be summarized by two main conclusions.

1. The seasonal cycle amplitude of CO_2 roughly follows surfaces of constant potential temperature, rather than pressure surfaces. Thus, isentropic transport is the fundamental reason for the latitudinal gradient of increasing CO_2 seasonal cycle amplitude along pressure surfaces throughout the troposphere, given the present-day latitudinal distribution of CO_2 emissions.
2. Since changes in the seasonal cycle amplitude follow surfaces of constant potential temperature, increasing seasonal fluxes in lower latitudes (i.e., temperate and boreal regions) have a larger impact on the seasonal cycle amplitude of CO_2 throughout most of the troposphere compared to increasing seasonal fluxes in higher latitudes (i.e., Arctic region). That is, amplification of surface flux seasonality at 30°N has a bigger effect than an equivalent amplification at 60°N when observed at 70°N, where SCA has been observed since the early 1960s at Barrow, Alaska.

In support of a dominant role of isentropic transport in carrying the seasonal cycle amplitude from the midlatitude surface to the Arctic, we find that the seasonal cycle amplitude of CO_2 increases with latitude independent of Arctic surface fluxes. Specifically, transport from lower latitudes accounts for approximately 60% of the northern high-latitude seasonal cycle even in the presence of a strongly seasonal Arctic biosphere. These results support the hypothesis that recently observed increasing CO_2 seasonal cycle amplitude at the surface and throughout the middle troposphere in northern high latitudes [e.g., *Graven et al.*, 2013; *Forkel et al.*, 2016; *Zeng et al.*, 2014] is likely driven by changes in midlatitude surface fluxes (i.e., temperature ecosystems), rather than changes in the Arctic. Our results demonstrate the critical importance of advective fluxes from much lower latitudes in controlling seasonal variations of CO_2 over Boreal and Arctic latitudes, especially aloft. Regional inverse models must include accurate specification of meridional transport by individual synoptic events as lateral boundary conditions [*Chang et al.*, 2014; *Henderson et al.*, 2015; *Karion et al.*, 2015].

The above conclusions are supported by tracer experiments in an idealized aquaplanet with no topography but are also reproduced by experiments with GEOS-Chem which includes topography and where transport is driven by reanalysis winds. Agreement between these two very different models points to a fundamental relationship between the periodic surface fluxes of any tracer and its high-latitude concentrations. That such a simplified aquaplanet can reproduce the observed latitudinal gradient in the seasonal cycle amplitude of CO_2 along pressure surfaces suggests that transport by synoptic eddies alone can account for this behavior.

It is well known that the distribution of atmospheric trace gases is strongly influenced by convective activity [*Denning et al.*, 1996], especially along the midlatitude storm tracks where vertical mixing is significantly enhanced by synoptic eddies and moist convective processes [*Miyazaki et al.*, 2008; *Parazoo et al.*, 2011, 2012]. Quantitative estimation of surface fluxes using modern atmospheric transport models includes these transport processes, but meridional transport in synoptic weather systems includes fine-scale mechanisms like frontal lifting and vertical motion in clouds that are unresolved by global models. Cloud permitting climate models produce more realistic vertical gradients of passive tracers compared to models utilizing conventional convective parameterizations [e.g., *Rosa et al.*, 2012] and drive enhanced poleward transport of trace gases from midlatitude source regions [*Wang et al.*, 2011]. Thus, it is likely that the estimates in this study, which are derived from two models that do not explicitly resolve convective processes, underestimate the influence of isentropic transport and hence the seasonal cycle amplitude of CO_2 in the midtroposphere. Future work should consider the effect of resolved convection, with careful analysis of transport on dry versus moist isentropic surfaces.

Appendix A

The gray-radiation aquaplanet of *Frierson et al.* [2006] does not include a seasonal cycle by default and is typically run under equinoctial conditions. Thus, here we will briefly describe how a 360 day seasonal cycle was simulated. First, the model computes the top-of-atmosphere average daily insolation according to the formula provided in equation (2.17) of *Hartmann* [1994]. However, the resulting seasonal cycle of the circulation is very unrealistic, with much too strong of a seasonality, e.g., the summer time jet stream and storm track lie poleward of 60°N. To make the seasonal cycle more realistic, we modify the default parameters of *Frierson et al.* [2006] and follow *Afargan and Kaspi* [2016] by defining a top-of-atmosphere (TOA) albedo:

$$\alpha_{\mathrm{TOA}} = \alpha_{\mathrm{TOA}_0} + \left(\alpha_{\mathrm{TOA}_1} - \alpha_{\mathrm{TOA}_0}\right) \cdot \sin(\theta)^4, \tag{A1}$$

where θ is degrees latitude, where $\alpha_{TOA_0} = 0.05$ and $\alpha_{TOA_1} = 0.45$. Then, the net downward solar radiation is multiplied by $(1 - \alpha_{TOA})$ to partially mute the default seasonal cycle. Finally, the surface longwave atmospheric optical depths at equator and pole (which approximate the effects of water vapor) [*Frierson et al.*, 2006, equation (4)] are modified to be $\tau_{0e} = 16.0$ and $\tau_{0p} = 8.0$. We note that while these modifications to the default parameters result in a more realistic seasonal cycle of the circulation, the general conclusions of this work would remain the same if the default parameters were used instead.

Acknowledgments
The authors would like to thank three anonymous reviewers for their helpful comments on an earlier version of this manuscript. E.A.B. was supported by the Climate and Large-scale Dynamics Program of the National Science Foundation under grant 1419818. A.S.D. gratefully acknowledges support from NASA's Science Mission Directorate under the Atmospheric Carbon Transport project (NNX15AJ09G). Part of the research in this study was performed at the Jet Propulsion Laboratory, California Institute of Technology, under contract with the National Aeronautics and Space Administration. We thank C. Koven for providing CLM4.5 CO2 surface flux fields, and the ODIAC fossil fuel CO_2 emissions were provided by T. Oda. The model output supporting the conclusions of this article is available from the corresponding author upon request (eabarnes@atmos.colostate.edu).

References

Afargan, H., and Y. Kaspi (2016), *A Midwinter Minimum in Storm Track Activity in an Idealized GCM With a Seasonal Cycle*, EGU General Assembly, Vienna, Austria.

Arora, V. K., et al. (2013), Carbon–concentration and carbon–climate feedbacks in CMIP5 Earth system models, *J. Clim.*, *26*(15), 5289–5314.

Bacastow, R., and C. Keeling (1981), Atmospheric carbon dioxide concentration and the observed airborne fraction, *Carbon cycle Model., SCOPE*, *16*, 103–112.

Bakwin, P., K. Davis, C. Yi, S. Wofsy, J. Munger, L. Haszpra, and Z. Barcza (2004), Regional carbon dioxide fluxes from mixing ratio data, *Tellus Ser. B*, *56*(4), 301–311.

Barth, M., et al. (2007), Cloud-scale model intercomparison of chemical constituent transport in deep convection, *Atmos. Chem. Phys.*, *7*(18), 4709–4731.

Bey, I., D. J. Jacob, R. M. Yantosca, J. A. Logan, B. Field, A. M. Fiore, Q. Li, H. Liu, L. J. Mickley, and M. Schultz (2001), Global modeling of tropospheric chemistry with assimilated meteorology: Model description and evaluation, *J. Geophys. Res.*, *106*(114), 23,073–23,096.

Chang, R. Y.-W., et al. (2014), Methane emissions from alaska in 2012 from carve airborne observations, *Proc. Natl. Acad. Sci.*, *111*(47), 16,694–16,699.

Corbin, K., A. Denning, and N. Parazoo (2009), Assessing temporal clear-sky errors in assimilation of satellite CO_2 retrievals using a global transport model, *Atmos. Chem. Phys.*, *9*(9), 3043–3048.

Cox, P. M., R. Betts, M. Collins, P. Harris, C. Huntingford, and C. Jones (2004), Amazonian forest dieback under climate-carbon cycle projections for the 21st century, *Theor. Appl. Climatol.*, *78*(1–3), 137–156.

Cramer, W., et al. (2001), Global response of terrestrial ecosystem structure and function to CO_2 and climate change: Results from six dynamic global vegetation models, *Global Change Biol.*, *7*(4), 357–373.

Crawford, J., et al. (2003), Clouds and trace gas distributions during TRACE-P, *J. Geophys. Res.*, *108*(21), 8818, doi:10.1029/2002JD003177.

Denning, A. S., D. A. Randall, G. J. Collatz, and P. J. Sellers (1996), Simulations of terrestrial carbon metabolism and atmospheric CO_2 in a general circulation model. Part 2: Simulated CO_2 concentrations, *Tellus Ser. B*, *48*(4), 542–567.

Dlugokencky, E., K. Masarie, P. Lang, and P. Tans (2015), NOAA Greenhouse Gas Reference from Atmospheric Carbon Dioxide Dry Air Mole Fractions from the NOAA ESRL Carbon Cycle Cooperative Global Air Sampling Network. [Available at ftp://aftp.cmdl.noaa.gov/data/trace_gases/co2/flask/surface/.]

Fisher, J. B., et al. (2014a), Carbon cycle uncertainty in the Alaskan Arctic, *Biogeosciences*, *11*, 4271–4288.

Fisher, J. B., D. N. Huntzinger, C. R. Schwalm, and S. Sitch (2014b), Modeling the terrestrial biosphere, *Annu. Rev. Environ. Resour.*, *39*, 91–123.

Forkel, M., N. Carvalhais, C. Rödenbeck, R. Keeling, M. Heimann, K. Thonicke, S. Zaehle, and M. Reichstein (2016), Enhanced seasonal CO_2 exchange caused by amplified plant productivity in northern ecosystems, *Science*, *4971*, 1–9, doi:10.1126/science.aac4971.

Frierson, D. M. W., I. M. Held, and P. Zurita-Gator (2006), A gray-radiation aquaplanet moist GCM: Static stability and eddy scale, *J. Atmos. Sci.*, *63*, 2548–2566.

Fung, I., K. Prentice, E. Matthews, J. Lerner, and G. Russell (1983), Three-dimensional tracer model study of atmospheric CO_2: Response to seasonal exchanges with the terrestrial biosphere, *J. Geophys. Res.*, *88*(C2), 1281–1294.

Fung, I., C. Tucker, and K. Prentice (1987), Application of advanced very high resolution radiometer vegetation index to study atmosphere-biosphere exchange of CO_2, *J. Geophys. Res.*, *92*(D3), 2999–3015.

Graven, H. D., et al. (2013), Enhanced seasonal exchange of CO_2 by Northern Ecosystems since 1960, *Science*, *341*(6150), 1085–1089, doi:10.1126/science.1239207.

Gray, J. M., S. Frolking, E. A. Kort, D. K. Ray, C. J. Kucharik, N. Ramankutty, and M. A. Friedl (2014), Direct human influence on atmospheric CO_2 seasonality from increased cropland productivity, *Nature*, *515*(7527), 398–401.

Gregory, J. M., C. Jones, P. Cadule, and P. Friedlingstein (2009), Quantifying carbon cycle feedbacks, *J. Clim.*, *22*(19), 5232–5250.

Harris, I., P. D. Jones, T. J. Osborn, and D. H. Lister (2014), Updated high-resolution grids of monthly climatic observations—The CRU TS3.10 Dataset, *Int. J. Climatol.*, *34*(3), 623–642, doi:10.1002/joc.3711.

Hartmann, D. L. (1994), *Global Physical Climatology*, vol. 56, 411 pp., Academic Press, San Diego, Calif.

Helliker, B. R., J. A. Berry, A. K. Betts, P. S. Bakwin, K. J. Davis, A. S. Denning, J. R. Ehleringer, J. B. Miller, M. P. Butler, and D. M. Ricciuto (2004), Estimates of net CO_2 flux by application of equilibrium boundary layer concepts to CO_2 and water vapor measurements from a tall tower, *J. Geophys. Res.*, *109*(D20), D20106, doi:10.1029/2004JD004532.

Henderson, J., et al. (2015), Atmospheric transport simulations in support of the Carbon in Arctic Reservoirs Vulnerability Experiment (CARVE), *Atmos. Chem. Phys.*, *15*(8), 4093–4116.

Hoffman, F., et al. (2014), Causes and implications of persistent atmospheric carbon dioxide biases in Earth system models, *J. Geophys. Res. Biogeosci.*, *119*, 141–162, doi:10.1002/2013JG002381.

Hopkins, F. M., M. S. Torn, and S. E. Trumbore (2012), Warming accelerates decomposition of decades-old carbon in forest soils, *Proc. Natl. Acad. Sci.*, *109*(26), E1753—E1761.

Huntzinger, D. N., et al. (2013), The north american carbon program multi-scale synthesis and terrestrial model intercomparison project—Part 1: Overview and experimental design, *Geosci. Model Dev.*, *6*(6), 2121–2133.

Hurwitz, M. D., D. M. Ricciuto, P. S. Bakwin, K. J. Davis, W. Wang, C. Yi, and M. P. Butler (2004), Transport of carbon dioxide in the presence of storm systems over a Northern Wisconsin forest, *J. Atmos. Sci.*, *61*(5), 607–618.

Kalnay, E., et al. (1996), The NCEP/NCAR 40-year reanalysis project, *Bull. Am. Meteorol. Soc.*, *83*, 437–471.

Karion, A., et al. (2015), Investigating alaskan methane and carbon dioxide fluxes using measurements from the CARVE tower, *Atmos. Chem. Phys. Discuss.*, *15*(23), 34,871–34,911.

Keeling, C. D. (1960), The concentration and isotopic abundances of carbon dioxide in the atmosphere, *Tellus*, *12*(2), 200–203.

Keppel-Aleks, G., P. O. Wennberg, and T. Schneider (2011), Sources of variations in total column carbon dioxide, *Atmos. Chem. Phys.*, *11*(8), 3581–3593, doi:10.5194/acp-11-3581-2011.

Keppel-Aleks, G., et al. (2012), The imprint of surface fluxes and transport on variations in total column carbon dioxide, *Biogeosciences*, *9*(3), 875–891, doi:10.5194/bg-9-875-2012.
Klonecki, A., P. Hess, L. Emmons, L. Smith, J. Orlando, and D. Blake (2003), Seasonal changes in the transport of pollutants into the Arctic troposphere-model study, *J. Geophys. Res.*, *108*(D4), 8367, doi:10.1029/2002JD002199.
Lagenhorst, A. (2005), Spectral Atmospheric Core Documentation, Tech. Rep., Geophysical Fluid Dynamics Laboratory, Princeton, N. J.
Le Quéré, C., et al. (2015), Global carbon budget 2014, *Earth Syst. Sci. Data*, *7*, 47–85.
LeBauer, D. S., and K. K. Treseder (2008), Nitrogen limitation of net primary productivity in terrestrial ecosystems is globally distributed, *Ecology*, *89*, and 371–379.
Lin, S., and R. Rood (1996), Multidimensional flux-form semi-Lagrangian transport schemes, *Mon. Weather Rev.*, *124*, 2046–2070, doi:10.1175/1520-0493.
Luo, Y., D. Hui, and D. Zhang (2006), Elevated CO_2 stimulates net accumulations of carbon and nitrogen in land ecosystems: A meta-analysis, *Ecology*, *87*(1), 53–63.
Messerschmidt, J., N. Parazoo, D. Wunch, N. M. Deutscher, C. Roehl, T. Warneke, and P. O. Wennberg (2013), Evaluation of seasonal atmosphere-biosphere exchange estimations with TCCON measurements, *Atmos. Chem. Phys.*, *13*(10), 5103–5115, doi:10.5194/acp-13-5103-2013.
Miller, C. E., and S. J. Dinardo (2012), Carve: The Carbon in Arctic Reservoirs Vulnerability Experiment, in *IEEE Aerospace Conference*, pp. 1–17, IEEE, Big Sky, Mont., doi:10.1109/AERO.2012.6187026.
Miyazaki, K., P. Patra, M. Takigawa, T. Iwasaki, and T. Nakazawa (2008), Global-scale transport of carbon dioxide in the troposphere, *J. Geophys. Res.*, *113*, doi:10.1029/2007JD009557.
Nassar, R., et al. (2010), Modeling global atmospheric co$_2$ with improved emission inventories and co$_2$ production from the oxidation of other carbon species, *Geosci. Model Dev.*, *3*(2), 689–716, doi:10.5194/gmd-3-689-2010.
Oda, T., and S. Maksyutov (2011), A very high-resolution (1 km × 1 km) global fossil fuel CO_2 emission inventory derived using a point source database and satellite observations of nighttime lights, *Atmos. Chem. Phys.*, *11*, 543–556.
Oleson, K. W., et al. (2013), Technical description of version 4.5 of the Community Land Model (CLM), *Tech. Rep. NCAR/TN-503+STR*, NCAR, doi:10.5065/D6RR1W7M.
Orbe, C., M. Holzer, L. M. Polvani, and D. Waugh (2013), Air-mass origin as a diagnostic of tropospheric transport, *J. Geophys. Res. Atmos.*, *118*, 1459–1470, doi:10.1002/jgrd.50133.
Parazoo, N., A. Denning, S. Kawa, K. Corbin, R. Lokupitiya, and I. Baker (2008), Mechanisms for synoptic variations of atmospheric CO_2 in North America, South America and Europe, *Atmos. Chem. Phys.*, *8*(23), 7239–7254.
Parazoo, N. C., A. S. Denning, J. A. Berry, A. Wolf, D. A. Randall, S. R. Kawa, O. Pauluis, and S. C. Doney (2011), Moist synoptic transport of CO_2 along the mid-latitude storm track, *Geophys. Res. Lett.*, *38*, L09804, doi:10.1029/2011GL047238.
Parazoo, N. C., A. S. Denning, S. R. Kawa, S. Pawson, and R. Lokupitiya (2012), CO_2 flux estimation errors associated with moist atmospheric processes, *Atmos. Chem. Phys.*, *12*(14), 6405–6416, doi:10.5194/acp-12-6405-2012.
Parazoo, N. C., et al. (2013), Interpreting seasonal changes in the carbon balance of southern Amazonia using measurements of XCO_2 and chlorophyll fluorescence from GOSAT, *Geophys. Res. Lett.*, *40*, 2829–2833, doi:10.1002/grl.50452.
Parazoo, N. C., R. Commane, S. Wofsy, C. Koven, C. Sweeney, D. Lawrence, J. Lindaas, R. Y.-W. Chang, and C. E. Miller (2016), Detecting patterns of changing CO_2 flux in Alaska, *Proc. Natl. Acad. Sci. U.S.A.*, doi:10.1073/pnas.1601085113.
Pauluis, O., A. Czaja, and R. Korty (2010), The global atmospheric circulation in moist isentropic coordinates, *J. Clim.*, *23*(11), 3077–3093.
Pearman, G., and P. Hyson (1980), Activities of the global biosphere as reflected in atmospheric CO_2 records, *J. Geophys. Res. Oceans*, *85*(C8), 4457–4467.
Randerson, J. T., M. V. Thompson, T. J. Conway, I. Y. Fung, and C. B. Field (1997), The contribution of terrestrial sources and sinks to trends in the seasonal cycle of atmospheric carbon dioxide, *Global Biogeochem. Cycles*, *11*(4), 535–560.
Rosa, D., J. F. Lamarque, and W. D. Collins (2012), Global transport of passive tracers in conventional and superparameterized climate models: Evaluation of multi-scale methods, *J. Adv. Model. Earth Systems*, *4*(10), M10003, doi:10.1029/2012MS000206.
Schuur, E., et al. (2013), Expert assessment of vulnerability of permafrost carbon to climate change, *Clim. Change*, *119*(2), 359–374, doi:10.1007/s10584-013-0730-7.
Shevliakova, E., S. W. Pacala, S. Malyshev, G. C. Hurtt, P. Milly, J. P. Caspersen, L. T. Sentman, J. P. Fisk, C. Wirth, and C. Crevoisier (2009), Carbon cycling under 300 years of land use change: Importance of the secondary vegetation sink, *Global Biogeochem. Cycles*, *23*, GB2022, doi:10.1029/2007GB003176.
Stohl, A. (2006), Characteristics of atmospheric transport into the Arctic troposphere, *J. Geophys. Res.*, *111*, D11306, doi:10.1029/2005JD006888.
Takahashi, T., et al. (2009), Climatological mean and decadal change in surface ocean pCO_2, and net sea-air CO_2 flux over the global oceans, *Deep Sea Res. Part II*, *56*(8-10), 554–577, doi:10.1016/j.dsr2.2008.12.009.
Tian, H., et al. (2015), Global patterns and controls of soil organic carbon dynamics as simulated by multiple terrestrial biosphere models: Current status and future directions, *Global Biogeochem. Cycles*, *29*, 775–792, doi:10.1002/2014GB005021.
Wang, M., S. Ghan, M. Ovchinnikov, X. Liu, R. Easter, E. Kassianov, Y. Qian, and H. Morrison (2011), Aerosol indirect effects in a multi-scale aerosol-climate model PNNL-MMF, *Atmos. Chem. Phys.*, *11*(11), 5431–5455, doi:10.5194/acp-11-5431-2011.
Wenzel, S., P. M. Cox, V. Eyring, and P. Friedlingstein (2014), Emergent constraints on climate-carbon cycle feedbacks in the CMIP5 Earth system models, *J. Geophys. Res. Biogeosci.*, *119*, 794–807, doi:10.1002/2013JG002591.
Wunch, D., et al. (2013), The covariation of Northern Hemisphere summertime CO_2 with surface temperature in boreal regions, *Atmos. Chem. Phys.*, *13*(18), 9447–9459, doi:10.5194/acp-13-9447-2013.
Zeng, N., F. Zhao, G. J. Collatz, E. Kalnay, R. J. Salawitch, T. O. West, and L. Guanter (2014), Agricultural Green Revolution as a driver of increasing atmospheric CO_2 seasonal amplitude, *Nature*, *515*(7527), 394–397, doi:10.1038/nature13893.